




Cite this: *Dalton Trans.*, 2019, **48**, 446Phosphane tuning in heteroleptic  $[\text{Cu}(\text{N}^{\wedge}\text{N})(\text{P}^{\wedge}\text{P})]^+$  complexes for light-emitting electrochemical cells†Fabian Brunner, <sup>a</sup> Azin Babaei, <sup>b</sup> Antonio Pertegás, <sup>b</sup> José M. Junquera-Hernández, <sup>b</sup> Alessandro Prescimone, <sup>a</sup> Edwin C. Constable, <sup>a</sup> Henk J. Bolink, <sup>b</sup> Michele Sessolo, <sup>\*b</sup> Enrique Ortí <sup>\*b</sup> and Catherine E. Housecroft <sup>\*a</sup>

The synthesis and characterization of five  $[\text{Cu}(\text{P}^{\wedge}\text{P})(\text{N}^{\wedge}\text{N})][\text{PF}_6]$  complexes in which  $\text{P}^{\wedge}\text{P}$  = 2,7-bis(*tert*-butyl)-4,5-bis(diphenylphosphino)-9,9-dimethylxanthene ( ${}^t\text{Bu}_2\text{xantphos}$ ) or the chiral 4,5-bis(mesitylphenylphosphino)-9,9-dimethylxanthene ( $\text{xantphosMes}_2$ ) and  $\text{N}^{\wedge}\text{N}$  = 2,2'-bipyridine (bpy), 6-methyl-2,2'-bipyridine (6-Mebpy) or 6,6'-dimethyl-2,2'-bipyridine (6,6'-Me<sub>2</sub>bpy) are reported. Single crystal structures of four of the compounds confirm that the copper(II) centre is in a distorted tetrahedral environment. In  $[\text{Cu}(\text{xantphosMes}_2)(6\text{-Mebpy})][\text{PF}_6]$ , the 6-Mebpy unit is disordered over two equally populated orientations and this disorder parallels a combination of two dynamic processes which we propose for  $[\text{Cu}(\text{xantphosMes}_2)(\text{N}^{\wedge}\text{N})]^+$  cations in solution. Density functional theory (DFT) calculations reveal that the energy difference between the two conformers observed in the solid-state structure of  $[\text{Cu}(\text{xantphosMes}_2)(6\text{-Mebpy})][\text{PF}_6]$  differ in energy by only 0.28 kcal mol<sup>-1</sup>. Upon excitation into the MLCT region ( $\lambda_{\text{exc}}$  = 365 nm), the  $[\text{Cu}(\text{P}^{\wedge}\text{P})(\text{N}^{\wedge}\text{N})][\text{PF}_6]$  compounds are yellow to orange emitters. Increasing the number of Me groups in the bpy unit shifts the emission to higher energies, and moves the Cu<sup>+</sup>/Cu<sup>2+</sup> oxidation to higher potentials. Photoluminescence quantum yields (PLQYs) of the compounds are low in solution, but in the solid state PLQYs of up to 59% (for  $[\text{Cu}({}^t\text{Bu}_2\text{xantphos})(6,6'\text{-Me}_2\text{bpy})]^+$ ) are observed. Increased excited-state lifetimes at low temperature are consistent with the complexes exhibiting thermally activated delayed fluorescence (TADF). This is supported by the small energy difference calculated between the lowest-energy singlet and triplet excited states (0.17–0.25 eV). The compounds were tested in simple bilayer light-emitting electrochemical cells (LECs). The optoelectronic performances of complexes containing  $\text{xantphosMes}_2$  were generally lower with respect to those with  ${}^t\text{Bu}_2\text{xantphos}$ , which led to bright and efficient devices. The best performing LECs were obtained for the complex  $[\text{Cu}({}^t\text{Bu}_2\text{xantphos})(6,6'\text{-Me}_2\text{bpy})][\text{PF}_6]$  due to the increased steric hindrance at the  $\text{N}^{\wedge}\text{N}$  ligand, resulting in higher PLQY.

Received 21st September 2018,  
Accepted 8th November 2018

DOI: 10.1039/c8dt03827a

rsc.li/dalton

## Introduction

Solid-state lighting technologies include organic-light emitting diodes (OLEDs) and light-emitting electrochemical cells

(LECs) and interest in these devices has grown tremendously in the last few years.<sup>1–4</sup> OLEDs are now well established and are widely employed in display applications. LECs feature many of the advantages of OLEDs including direct electron-to-photon conversion and the possibility of fabrication employing flexible surfaces and thin-film processing. Additionally, the simple device architecture of LECs and the use of air-stable electrode materials might reduce the manufacturing cost of electroluminescent devices and widen their field of applications.<sup>5–7</sup> LECs incorporating ionic transition-metal complexes (iTCs) based on iridium (and to a lesser extent ruthenium) have been the focus of intense investigations and show good performances in terms of colour tunability, brightness and device lifetime.<sup>8–14</sup> However, the limited availability of iridium and ruthenium in the Earth's crust motivated the search for alternative emissive materials.

<sup>a</sup>Department of Chemistry, University of Basel, Spitalstrasse 51, CH-4056 Basel, Switzerland. E-mail: catherine.housecroft@unibas.ch<sup>b</sup>Instituto de Ciencia Molecular, Universidad de Valencia, 46100 Paterna, Valencia, Spain. E-mail: enrique.orti@uv.es, michele.sessolo@uv.es

† Electronic supplementary information (ESI) available: Synthetic experimental details. Fig. S1, S2 and S6–S10: IR spectra of ligands and complexes. Fig. S3 and S11–S14: ORTEP-style plots of crystal structures. Fig. S4, S5 and S15–S22: additional NMR figures. Fig. S23 and S24: Solution absorption and emission spectra. Table S1: Selected structural parameters calculated at the B3LYP-D3/def2svp + def2tzvp level. CCDC 1844060–1844063 and 1860879. For ESI and crystallographic data in CIF or other electronic format see DOI: 10.1039/c8dt03827a



LECs were prepared on top of patterned indium tin oxide (ITO,  $15 \text{ } \Omega \text{ sq}^{-1}$ ) coated glass substrates previously cleaned by chemical and UV-ozone methods. Prior to the deposition of the emitting layer, 80 nm thick films of poly-(3,4-ethylenedioxythiophene):poly(styrenesulfonate) (PEDOT:PSS) (CLEVIOS™ P VP AI 4083, Heraeus) were coated in order to flatten the ITO electrode and to increase its work function. The emitting layer (100 nm thick) was prepared by spin-coating a dichloromethane solution of the emitting compound with the addition of the ionic liquid 1-ethyl-3-methylimidazolium hexafluorophosphate [Emim][PF<sub>6</sub>] (>98.5%, Sigma-Aldrich), in a 4 : 1 molar ratio. The devices were then transferred to an inert atmosphere glovebox (<0.1 ppm O<sub>2</sub> and H<sub>2</sub>O), where the aluminium cathode (100 nm) was thermally deposited in high

Data were collected on a Bruker Kappa Apex2 diffractometer with data reduction, solution and refinement using the programs APEX<sup>41</sup> and CRYSTALS.<sup>42</sup> Structural analysis was carried out using Mercury v. 3.7.<sup>43,44</sup> In [Cu(<sup>t</sup>Bu<sub>2</sub>xantphos)(6-Mebpy)][PF<sub>6</sub>].1.5CH<sub>2</sub>Cl<sub>2</sub>.0.5H<sub>2</sub>O, one CH<sub>2</sub>Cl<sub>2</sub> molecule was refined and SQUEEZE<sup>45</sup> was used to treat part of the solvent region; formulae and numbers were modified in the cif to keep this result into account. In [Cu(xantphosMes<sub>2</sub>)(6-Mebpy)][PF<sub>6</sub>], the 6-Mebpy is orientationally disordered over two orientations and the relevant aromatic rings were refined as rigid bodies.

C<sub>45</sub>H<sub>44</sub>OP<sub>2</sub>,  $M = 662.79$ , colourless plate, monoclinic, space group  $P2_1/n$ ,  $a = 10.6380(9)$ ,  $b = 15.0841(13)$ ,  $c = 23.545(2)$  Å,  $\beta = 102.585(3)^\circ$ ,  $U = 3687.4(5)$  Å<sup>3</sup>,  $Z = 4$ ,  $D_c = 1.194$  Mg m<sup>-3</sup>,  $\mu(\text{Cu-K}\alpha) = 1.317$  mm<sup>-1</sup>,  $T = 123$  K. Total 40 993 reflections, 6810 unique,  $R_{\text{int}} = 0.035$ . Refinement of 6264 reflections (433 parameters) with  $I > 2\sigma(I)$  converged at final  $R_1 = 0.0336$  ( $R_1$  all data = 0.0365),  $wR_2 = 0.0776$  ( $wR_2$  all data = 0.0794), GOF = 0.9775. CCDC 1860879.†

C<sub>59</sub>H<sub>61</sub>CuF<sub>6</sub>N<sub>2</sub>O<sub>1.5</sub>P<sub>3</sub>,  $M = 1092.60$ , yellow block, triclinic, space group  $P\bar{1}$ ,  $a = 12.0991(12)$ ,  $b = 13.3253(13)$ ,  $c = 18.6750(18)$  Å,  $\alpha = 91.353(3)$ ,  $\beta = 90.939(3)$ ,  $\gamma = 115.475(2)^\circ$ ,  $U = 2716.2(5)$  Å<sup>3</sup>,  $Z = 2$ ,  $D_c = 1.336$  Mg m<sup>-3</sup>,  $\mu(\text{Cu-K}\alpha) = 1.932$  mm<sup>-1</sup>,  $T = 123$  K. Total 35 686 reflections, 9826 unique,  $R_{\text{int}} = 0.029$ . Refinement of 9540 reflections (664 parameters) with  $I > 2\sigma(I)$  converged at final  $R_1 = 0.0416$  ( $R_1$  all data = 0.0423),  $wR_2 = 0.1012$  ( $wR_2$  all data = 0.1016),  $\text{gof} = 0.9707$ . CCDC 1844060.†

$\text{C}_{59.5}\text{H}_{62}\text{Cl}_3\text{CuF}_6\text{N}_2\text{O}_{1.5}\text{P}_3$ ,  $M = 1205.97$ , yellow block, triclinic, space group  $P\bar{1}$ ,  $a = 10.7080(9)$ ,  $b = 13.4475(12)$ ,  $c = 22.167(2)$  Å,  $\alpha = 73.142(6)$ ,  $\beta = 79.483(6)$ ,  $\gamma = 86.606(6)^\circ$ ,  $U = 3003.4(5)$  Å<sup>3</sup>,  $Z = 2$ ,  $D_c = 1.33$  Mg m<sup>-3</sup>,  $\mu(\text{Cu-K}\alpha) = 2.997$  mm<sup>-1</sup>,  $T = 123$  K. Total 35 561 reflections, 10 903 unique,  $R_{\text{int}} = 0.082$ . Refinement of 7619 reflections (700 parameters) with  $I > 2\sigma(I)$  converged at final  $R_1 = 0.1178$  ( $R_1$  all data = 0.1490),  $wR_2 = 0.1151$  ( $wR_2$  all data = 0.1470), GOF = 1.0317. CCDC 1844063.†

$\text{C}_{55}\text{H}_{52}\text{CuF}_6\text{N}_2\text{OP}_3$ ,  $M = 1027.49$ , yellow block, monoclinic, space group  $C2/c$ ,  $a = 38.341(2)$ ,  $b = 11.8342(7)$ ,  $c = 26.5208(14)$  Å,  $\beta = 126.4524(19)^\circ$ ,  $U = 9679.2(10)$  Å<sup>3</sup>,  $Z = 8$ ,  $D_c = 1.410$  Mg m<sup>-3</sup>,  $\mu(\text{Cu-K}\alpha) = 2.126$  mm<sup>-1</sup>,  $T = 123$  K. Total 29 726 reflections, 8726 unique,  $R_{\text{int}} = 0.027$ . Refinement of 7795 reflections (613 parameters) with  $I > 2\sigma(I)$  converged at final  $R_1 = 0.0320$

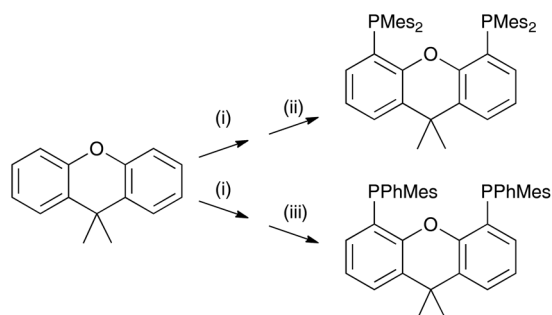
vacuum using an Edwards Auto500 chamber integrated in the glovebox. The thickness of all films was determined with an Ambios XP-1 profilometer. The active area of the devices was  $6.5 \text{ mm}^2$ . LECs were not encapsulated and were characterized inside the glovebox at room temperature. The device lifetime was measured by applying a pulsed current and monitoring the voltage and luminance *versus* time by a True Colour Sensor MAZeT (MTCSiCT Sensor) with a Botest OLT OLED Lifetime-Test System. The electroluminescence (EL) spectra were measured using an Avantes AvaSpec-2048 Fiber Optic Spectrometer during device lifetime measurement.

## Results and discussion

### Preparation and characterization of P<sup>^</sup>P ligands

The P<sup>^</sup>P ligand <sup>t</sup>Bu<sub>2</sub>xantphos was synthesized using the literature procedure.<sup>38</sup> The synthetic routes to xantphosMes<sub>4</sub> and xantphosMes<sub>2</sub> were based on the strategy of Hamann and Hartwig to prepare bidentate phosphanes with varying steric properties.<sup>59</sup> The syntheses of xantphosMes<sub>4</sub> and xantphosMes<sub>2</sub> are summarized in Scheme 2. Both compounds were isolated as white solids, but facile oxidation to the phosphane oxides made it difficult to obtain analytically pure samples. The electrospray (ESI) mass spectra of xantphosMes<sub>4</sub> and xantphosMes<sub>2</sub> showed base peaks at  $m/z$  747.3 and 663.5, respectively, arising from the  $[M + H]^+$  ions. The solid-state IR spectra of <sup>t</sup>Bu<sub>2</sub>xantphos and xantphosMes<sub>2</sub> are shown in Fig. S1 and S2.† Single crystals of xantphosMes<sub>2</sub> were grown from an Et<sub>2</sub>O solution of the compound by slow evaporation. Fig. S3† shows an ORTEP-style plot of the molecule and important bond parameters are given in the figure caption. Few chiral xantphos-derived ligands have been reported in the literature,<sup>60,61</sup> and the solid-state structure of xantphosMes<sub>2</sub> represents the (*rac*)-form of xantphosMes<sub>2</sub>. It crystallizes in the monoclinic  $P2_1/n$  space group with both the (*R,R*)- and (*S,S*)-enantiomers in the unit cell; the (*S,S*)-enantiomer is shown in Fig. 1. The xanthene unit deviates very slightly from planarity, in contrast to the 'bowl' shape that is commonly adopted (see discussion below).

The <sup>31</sup>P NMR spectra of xantphosMes<sub>4</sub> and xantphosMes<sub>2</sub> exhibit resonances at  $\delta$  −36.2 and −25.8 ppm, respectively,



**Scheme 2** Syntheses of xantphosMes<sub>4</sub> and xantphosMes<sub>2</sub>. Conditions: (i) <sup>t</sup>BuLi, dry heptane, TMEDA, reflux, 20 min; (ii) Mes<sub>2</sub>PCL, THF, 0 °C, 1 h; (iii) MesPhPCL, THF, 0 °C, 1 h.

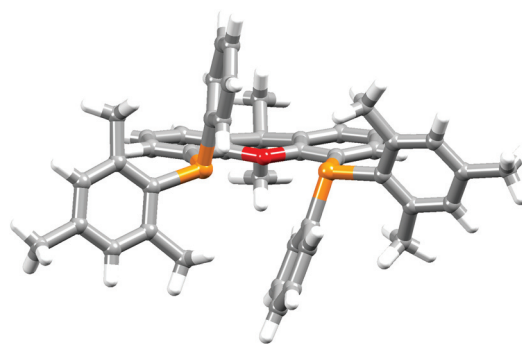


**Fig. 1** Crystallographically determined structure of the (*S,S*)-enantiomer of xantphosMes<sub>2</sub>. See also Fig. S3.†

consistent with one phosphorus environment in each compound. <sup>1</sup>H and <sup>13</sup>C NMR spectra (see Experimental section in the ESI†) were assigned by 2D methods and were in accord with functionalization in the 4,5-positions of the xanthene unit (Scheme 2). The <sup>1</sup>H NMR spectra are shown in Fig. S4 and S5.† The <sup>1</sup>H NMR spectrum of xantphosMes<sub>2</sub> (Fig. S5†) also shows the presence of a subspecies in solution, present in <10% based on integration. The chemical shifts of the low intensity signals and the presence of diagnostic NOESY peaks suggest the major and minor species are structurally related, and we assign them to the (*rac*)- and (*meso*)-forms, respectively. Based on the preference seen in the solid-state, we propose that the dominant species is the (*rac*)-form. Thus, the bisphosphane is preorganized to give particular diastereoisomers upon complexation with copper(i) and this indeed is the case as discussed later.

### Preparation and characterization of copper(i) complexes

Attempts to prepare [Cu(xantphosMes<sub>4</sub>)(bpy)][PF<sub>6</sub>], [Cu(xantphosMes<sub>4</sub>)(6-Mebpy)][PF<sub>6</sub>] and [Cu(xantphosMes<sub>4</sub>)(6,6'-Mebpy)][PF<sub>6</sub>] by reaction of [Cu(MeCN)<sub>4</sub>][PF<sub>6</sub>] and xantphosMes<sub>4</sub> followed by the corresponding 2,2'-bipyridine ligand failed to yield the desired heteroleptic complexes. The <sup>31</sup>P spectrum of each crude reaction mixture was dominated by a signal for the free ligand ( $\delta$  −36.2 ppm), and also exhibited several other unassigned signals. Evidence for the formation of [Cu(xantphosMes<sub>4</sub>)]<sup>+</sup> came from ESI mass spectrometry with a peak envelope at  $m/z$  809.5. Mononuclear [Cu(P<sup>^</sup>P)]<sup>+</sup> complexes containing sterically demanding substituents attached to the phosphorus atoms are known, for example [Cu(*t*Bu-xantphos- $\kappa^{P,O,P}$ )]<sup>+</sup>[PF<sub>6</sub>]<sup>37</sup> (*t*Bu-xantphos = 9,9-dimethyl-4,5-bis(di-*tert*-butylphosphino)xanthene) and 3-coordinate copper(i) complexes with P<sup>^</sup>N<sup>^</sup>P pincer ligands.<sup>62</sup> Since xantphosMes<sub>4</sub> proved to be too sterically demanding for the formation of [Cu(xantphosMes<sub>4</sub>)(N<sup>^</sup>N)]<sup>+</sup> species, we turned our attention to the use of xantphosMes<sub>2</sub>.

Heteroleptic [Cu(P<sup>^</sup>P)(N<sup>^</sup>N)]<sup>+</sup> complexes with P<sup>^</sup>P = <sup>t</sup>Bu<sub>2</sub>xantphos or xantphosMes<sub>2</sub> were prepared using the established procedure<sup>24</sup> by the addition of a mixture of the xantphos and bpy ligands to a solution of [Cu(MeCN)<sub>4</sub>][PF<sub>6</sub>] in





This journal is © The Royal Society of Chemistry 2019

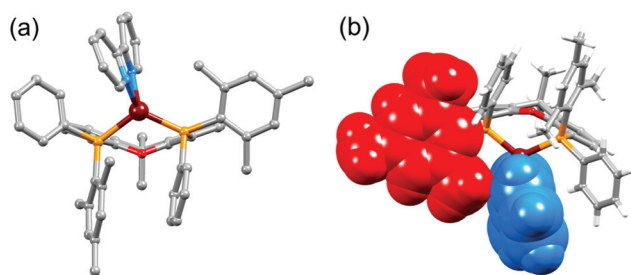


**Fig. 3** Structure of the  $[\text{Cu}(\text{xantphosMes}_2)(\text{bpy})]^+$  cation (a) emphasizing the relative positions of the phenyl and mesityl substituents with respect to the bpy unit, and (b) with the bpy (blue) and one mesityl group (red) shown in space-filling representation to emphasize their spatial proximity.

tionally disordered over two sites, each with 50% occupancy. Fig. 2b depicts the conformer in which the Me group is remote from the xanthene unit; the second conformer is structurally related to  $[\text{Cu}(\text{Bu}_2\text{xantphos})(6\text{-Meppy})]^+$  (Fig. 2a). The N–C–C–N torsion angles in Table 1 demonstrate that the bpy unit is significantly more twisted in the cations containing the xantphosMes<sub>2</sub> ligand than those with <sup>t</sup>Bu<sub>2</sub>xantphos. This appears to be associated with the fact that in both  $[\text{Cu}(\text{xantphosMes}_2)(\text{bpy})][\text{PF}_6]$  (Fig. 3) and  $[\text{Cu}(\text{xantphosMes}_2)(6\text{-Meppy})][\text{PF}_6]$  one methyl group of one mesityl substituent is directed towards the middle of the bpy domain (Fig. 3b). This spatial proximity is characterized by  $C_{\text{Me}(\text{Mes})}\cdots\text{centroid}_{\text{pyridine}}$  distances of 3.98 and 4.37 Å ( $H_{\text{Me}(\text{Mes})}\cdots\text{centroid}_{\text{pyridine}} = 3.16$  and 3.56 Å) in the  $[\text{Cu}(\text{xantphosMes}_2)(\text{bpy})]^+$  cation. Corresponding separations in  $[\text{Cu}(\text{xantphosMes}_2)(6\text{-Meppy})]^+$  are 4.00 and 4.38 Å (3.24 and 3.57 Å) and 3.85 and 4.39 Å (3.27 and 3.48 Å) for the two partial occupancy 6-Meppy sites.

### Solution NMR spectroscopy

The aromatic regions of the solution <sup>1</sup>H NMR spectra of  $[\text{Cu}(\text{Bu}_2\text{xantphos})(\text{bpy})][\text{PF}_6]$ ,  $[\text{Cu}(\text{xantphosMes}_2)(\text{bpy})][\text{PF}_6]$  and  $[\text{Cu}(\text{Bu}_2\text{xantphos})(6,6'\text{-Me}_2\text{bpy})][\text{PF}_6]$  are shown in Fig. 4 (see also Fig. S15<sup>†</sup>), S16 and S17,<sup>†</sup> respectively. All signals are sharp and well-resolved at room temperature and were assigned using COSY,

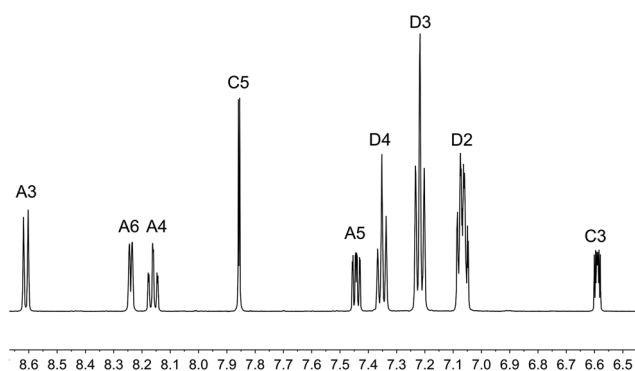


**Fig. 4** Aromatic region of the <sup>1</sup>H NMR spectrum (500 MHz, acetone-*d*<sub>6</sub>) of  $[\text{Cu}(\text{Bu}_2\text{xantphos})(\text{bpy})][\text{PF}_6]$ . See Fig. S15<sup>†</sup> for the full spectrum. See Scheme 3 for atom labelling.

NOESY, HMBC and HMQC methods. The <sup>t</sup>Bu substituents give rise to a singlet at  $\delta$  1.11 ppm in  $[\text{Cu}(\text{Bu}_2\text{xantphos})(\text{bpy})][\text{PF}_6]$  and  $\delta$  1.16 ppm in  $[\text{Cu}(\text{Bu}_2\text{xantphos})(6,6'\text{-Me}_2\text{bpy})][\text{PF}_6]$ . Fig. 4 and S16<sup>†</sup> reveal that the two pyridine rings of bpy in  $[\text{Cu}(\text{Bu}_2\text{xantphos})(\text{bpy})][\text{PF}_6]$  and  $[\text{Cu}(\text{xantphosMes}_2)(\text{bpy})][\text{PF}_6]$  are magnetically equivalent. Similarly, the 6,6'-Me<sub>2</sub>bpy ligand in  $[\text{Cu}(\text{Bu}_2\text{xantphos})(6,6'\text{-Me}_2\text{bpy})][\text{PF}_6]$  is symmetric on the NMR timescale at room temperature (Fig. S17<sup>†</sup>). We have previously detailed a solution dynamic behaviour for  $[\text{Cu}(\text{xantphos})(\text{N}^{\wedge}\text{N})]^+$  complexes involving inversion of the xanthene unit ('bowl'),<sup>26,32</sup> and this is depicted in the first dynamic process illustrated in Fig. 5. The scheme demonstrates that inversion of the xanthene bowl exchanges the environments of

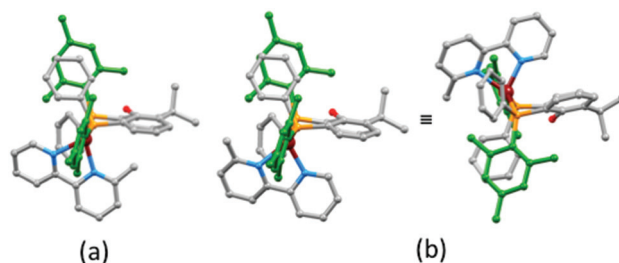
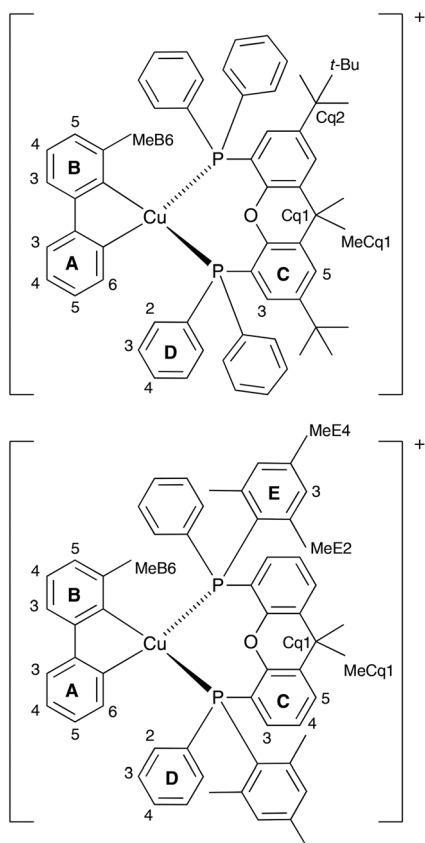


**Fig. 5** Upper: Proposed dynamic processes in  $[\text{Cu}(\text{xantphos})(\text{bpy})]^+$  type compounds.  $N_A$  and  $N_B$  represent pyridine rings A and B. For <sup>t</sup>Bu<sub>2</sub>xantphos,  $R_1 = R_2 = \text{Ph}$ . For xantphosMes<sub>2</sub>,  $R_1 = \text{Mes}$ ,  $R_2 = \text{Ph}$ . Lower: Crystallographically determined structure of the  $[\text{Cu}(\text{xantphosMes}_2)(6\text{-Meppy})]^+$  cation in which the 6-Meppy is orientationally disordered: (a) orientation 1 of 6-Meppy, and (b) orientation 2 of 6-Meppy shown in two views of the cation (see text).

the xanthphos methyl groups (green and magenta in Fig. 5) between axial and equatorial sites, but does not render pyridine rings A and B (represented by  $N_A$  and  $N_B$ ) equivalent. By invoking a second process involving movement of the  $\{Cu(bpy)\}$  unit (*i.e.*, a change in conformation of the chelate ring, Fig. 5),  $N_A$  and  $N_B$  experience both sides of the xanthene bowl and are equivalent on the NMR timescale.

On going from  $[Cu(^tBu_2xantphos)(bpy)][PF_6]$  to  $[Cu(^tBu_2xantphos)(6-Mebpy)][PF_6]$ , the symmetry of the cation is lowered and phenyl rings D (see Scheme 3) split into two sets, those proximate to the methyl group of 6-Mebpy and those on the side of the unsubstituted pyridine ring (Fig. 2a). Fig. 6 shows the aromatic region of the solution  $^1H$  NMR spectrum of  $[Cu(^tBu_2xantphos)(6-Mebpy)][PF_6]$ , in which the sets of D rings are labelled D and D'. In the NOESY spectrum at 298 K, exchange (EXSY) peaks are observed between pairs of signals for protons D2/D2' and D3/D3'; the D4/D4' EXSY peaks appear too close to the diagonal in the NOESY spectrum to be clearly resolved. NOESY cross peaks (no EXSY) are observed between MeCq1 and MeCq1' (Fig. S18†). These observations are consistent with inversion of the chelate ring ('copper flip' in Fig. 5) and no inversion of the xanthene bowl.

The single crystal structures of  $[Cu(xantphosMes_2)(bpy)][PF_6]$  and  $[Cu(xantphosMes_2)(6-Mebpy)][PF_6]$  reveal that



**Scheme 3** Structures of  $[Cu(^tBu_2xantphos)(6-Mebpy)]^+$  and  $[Cu(xantphosMes_2)(6-Mebpy)]^+$  with labelling for NMR spectroscopic assignments.

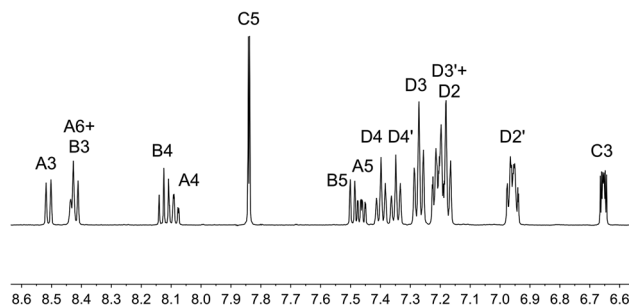


**Fig. 6** Aromatic region of the  $^1H$  NMR spectrum (500 MHz, acetone- $d_6$ ) of  $[Cu(^tBu_2xantphos)(6-Mebpy)][PF_6]$ . See Scheme 3 for atom labelling.

the two PPhMes groups of the xantphosMes<sub>2</sub> ligand are mutually oriented as shown in Fig. 3a and 5. This desymmetrizes the xanthene unit (labelled rings C and C'). In addition, the equatorial and axial positions of the Ph and Mes substituents with respect to the chelate ring leads to chemical shift differences in the  $^1H$  NMR spectrum for pairs of phenyl rings (D and D') and mesityl groups (E and E'). Fig. S19† shows the  $^1H$  NMR spectrum of  $[Cu(xantphosMes_2)(6-Mebpy)][PF_6]$ , and Fig. 7 and S20† show exchange peaks observed in the NOESY spectrum. Exchange peaks between the signals for phenyl proton D2/D2' and D4/D4' is consistent with the 'copper flip' shown in Fig. 5. This leads to equivalence of the outer rings of the xanthene unit as confirmed by the EXSY peak between the signals for protons C3/C3'. The EXSY peak between signals for the xanthene methyls MeCq1 and MeCq1' (Fig. S20†) confirms the inversion of the xanthene bowl (Fig. 5). This contrasts with  $[Cu(^tBu_2xantphos)(6-Mebpy)][PF_6]$  where no exchange (only NOESY) peaks are observed (see above and Fig. S18†).

Earlier, we noted an orientational disorder of the 6-Mebpy ligand in the solid-state structure of  $[Cu(xantphosMes_2)]$

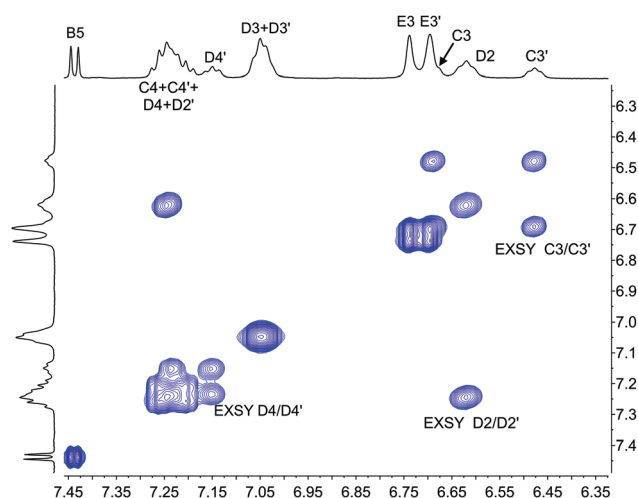


**Fig. 7** Part of the NOESY spectrum (500 MHz, acetone- $d_6$ ) of  $[Cu(xantphosMes_2)(6-Mebpy)][PF_6]$  showing exchange (EXSY) peaks between pairs of protons C3 and C3', D2 and D2', and D4 and D4'. See also Fig. S20†.



(6-Mebpy)][PF<sub>6</sub>]. The disorder was modelled with a 50% occupancy of each orientation and Fig. 5a and b show the [Cu(xantphosMes<sub>2</sub>)(6-Mebpy)]<sup>+</sup> with the two orientations of 6-Mebpy. The structure in Fig. 5a corresponds to the top diagram in the scheme in Fig. 5, while Fig. 5b corresponds to the bottom diagram in the scheme. The disorder therefore parallels a combination of the two dynamic processes which we propose the cation undergoes in solution.

Variable temperature (VT) NMR spectra were recorded for an acetone-*d*<sub>6</sub> solution of [Cu(xantphosMes<sub>2</sub>)(6-Mebpy)][PF<sub>6</sub>]. The <sup>31</sup>P NMR spectrum (Fig. S21†) shows only one signal over the range 298–180 K. Fig. 8 shows the effect of temperature on the alkyl region of the <sup>1</sup>H NMR spectrum of [Cu(xantphosMes<sub>2</sub>)(6-Mebpy)][PF<sub>6</sub>]. The collapse of the signals for mesityl-methyl protons MeE2 and MeE2' and the appearance of four signals for these methyls below 218 K are consistent with freezing out the rotation of the mesityl groups. A similar temperature dependence is observed for the mesityl E3 protons in the aromatic region of the spectrum (Fig. S22†). Significant shifting of the xanthene methyl protons MeCq1 and MeCq1' (Fig. 8) and 6-Mebpy protons A6 and MeB6 (Fig. S22†) can be attributed to changes in their magnetic environments as the mesityl groups adopt a static configuration. Both <sup>31</sup>P and <sup>1</sup>H VT NMR spectra are consistent with the presence of only one conformer in solution.

## Electrochemistry

The electrochemical behaviour of the [Cu(N<sup>^</sup>N)(P<sup>^</sup>P)][PF<sub>6</sub>] complexes was studied using cyclic voltammetry and the results are summarized in Table 2 and Fig. 9. All compounds with the exception of [Cu(xantphosMes<sub>2</sub>)(bpy)][PF<sub>6</sub>] exhibit a quasi-reversible process in the range +0.76 to +0.85 V, which is assigned to a copper-centred oxidation. For [Cu(xantphosMes<sub>2</sub>)(bpy)][PF<sub>6</sub>] the oxidation at +0.80 V is irreversible. Although the corresponding reduction peak could not be resolved, the position of this oxidation peak (*E*<sub>pc</sub><sup>ox</sup>) is similar the one observed for [Cu(<sup>t</sup>Bu<sub>2</sub>xantphos)(bpy)][PF<sub>6</sub>] (+0.80 V, Fig. 9).

**Table 2** Cyclic voltammetric data for [Cu(N<sup>^</sup>N)(P<sup>^</sup>P)][PF<sub>6</sub>] complexes referenced to internal Fc/Fc<sup>+</sup> = 0 V; degassed HPLC grade CH<sub>2</sub>Cl<sub>2</sub> solution with [Bu<sub>4</sub>N][PF<sub>6</sub>] as supporting electrolyte and a scan rate of 0.1 V s<sup>−1</sup>. Processes are quasi reversible unless otherwise stated (ir = irreversible). Data for [Cu(xantphos)(N<sup>^</sup>N)][PF<sub>6</sub>] (N<sup>^</sup>N = bpy, 6-Mebpy, 6,6'-Me<sub>2</sub>bpy) are also included

Complex cation	<i>E</i> <sub>1/2</sub> <sup>ox</sup> /V ( <i>E</i> <sub>pc</sub> − <i>E</i> <sub>pa</sub> /mV)	<i>E</i> <sub>pc</sub> <sup>ox</sup> /V	<i>E</i> <sub>pa</sub> <sup>red</sup> /V
[Cu( <sup>t</sup> Bu <sub>2</sub> xantphos)(bpy)] <sup>+</sup>	+0.76 (90)		−2.20
[Cu( <sup>t</sup> Bu <sub>2</sub> xantphos)(6-Mebpy)] <sup>+</sup>	+0.83 (90)		−2.22
[Cu( <sup>t</sup> Bu <sub>2</sub> xantphos)(6,6'-Me <sub>2</sub> bpy)] <sup>+</sup>	+0.85 (100)		−2.28
[Cu(xantphosMes <sub>2</sub> )(bpy)] <sup>+</sup>		+0.80 <sup>ir</sup>	
[Cu(xantphosMes <sub>2</sub> )(6-Mebpy)] <sup>+</sup>	+0.84 (70)		
[Cu(xantphos)(bpy)] <sup>+</sup> <sup>a</sup>	+0.76 (110)		
[Cu(xantphos)(6-Mebpy)] <sup>+</sup> <sup>a</sup>	+0.85 (100)		
[Cu(xantphos)(6,6'-Me <sub>2</sub> bpy)] <sup>+</sup> <sup>a</sup>	+0.90 (150)		

<sup>a</sup> Values taken from ref. 24.

When scanning beyond +1.0 V, additional oxidation waves appear and the copper oxidation is no longer reversible. Instead a reduction signal appears at around +0.25 V. This indicates decomposition of the complexes at potentials higher than +1.0 V. Complexes containing <sup>t</sup>Bu<sub>2</sub>xantphos also show an irreversible reduction wave at around −2.2 V (Table 2) arising from a ligand-based process. For the complexes containing xantphosMes<sub>2</sub>, no reduction processes were observed within the solvent accessible window.

Along the series [Cu(<sup>t</sup>Bu<sub>2</sub>xantphos)(N<sup>^</sup>N)][PF<sub>6</sub>] with N<sup>^</sup>N = bpy to 6-Mebpy to 6,6'-Me<sub>2</sub>bpy, the copper oxidation shifts to higher potentials (as observed for the analogous [Cu(xantphos)(N<sup>^</sup>N)][PF<sub>6</sub>] series, Table 2<sup>24</sup>) while the reduction moves towards more negative potentials. This demonstrates an increase in the HOMO–LUMO gap as the steric demand of the bpy ligand increases. This trend was also observed for a related series of compounds and has been rationalized using DFT calculations.<sup>24</sup>



**Fig. 8** Alkyl regions of the variable temperature <sup>1</sup>H NMR spectra (500 MHz, acetone-*d*<sub>6</sub>) of [Cu(xantphosMes<sub>2</sub>)(6-Mebpy)][PF<sub>6</sub>]. See Scheme 3 for atom labelling.

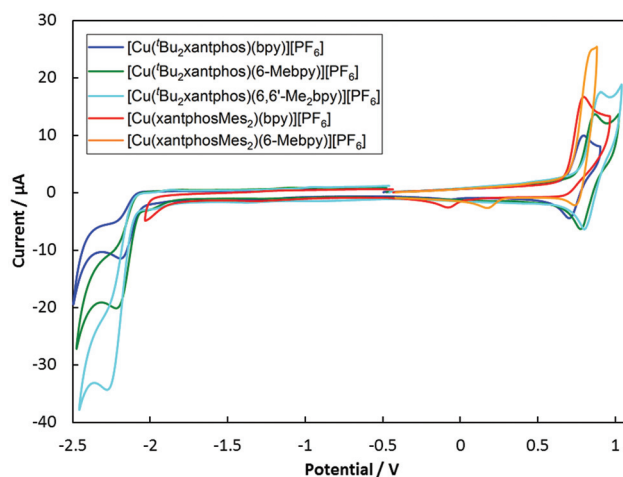


**Fig. 9** Cyclic voltammograms of [Cu(P<sup>^</sup>P)(N<sup>^</sup>N)][PF<sub>6</sub>] compounds in CH<sub>2</sub>Cl<sub>2</sub> at a scan rate of 100 mV s<sup>−1</sup> referenced to internal Fc/Fc<sup>+</sup> = 0 V.







Dalton Trans., 2019, 48, 446–460 | 455

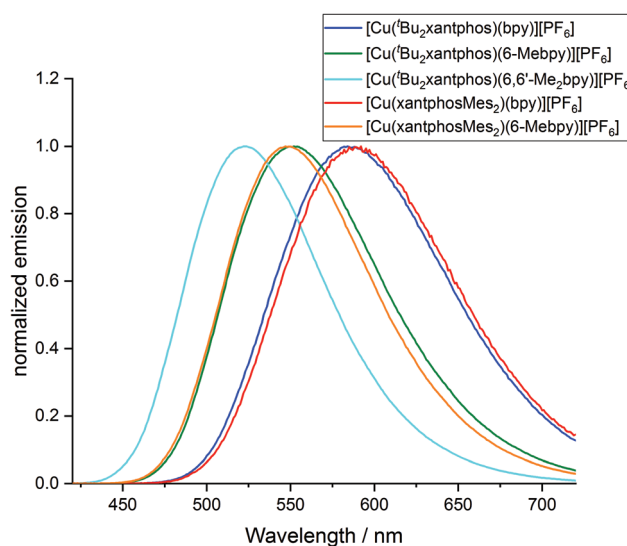
**Table 3** Photophysical properties of the [Cu(P<sup>^</sup>AP)(N<sup>^</sup>N)](PF<sub>6</sub>) complexes compared to [Cu(xantphos)(N<sup>^</sup>N)](PF<sub>6</sub>) (N<sup>^</sup>N = bpy, 6-Mebpy, 6,6'-Me<sub>2</sub>bpy)

Complex cation	CH <sub>2</sub> Cl <sub>2</sub> solution <sup>a,b</sup>				Powder <sup>d</sup>				Me-THF at 77 K				Thin film	
	UV-Vis MLCT λ <sub>max</sub> /nm	λ <sub>em</sub> <sup>max</sup> /nm	PLQY (non-degassed)/ degassed/%	τ <sub>1/2</sub> (av) <sup>a,b</sup> / degassed/μs	λ <sub>em</sub> <sup>max</sup> /nm	PLQY/%	τ <sub>1/2</sub> (av) <sup>a,b</sup> / μs	λ <sub>em</sub> <sup>max</sup> /nm	PLQY/%	λ <sub>em</sub> <sup>max</sup> /nm	PLQY/%	τ <sub>1/2</sub> (av) <sup>a,b</sup> / μs	λ <sub>em</sub> <sup>max</sup> /nm	PLQY/%
[Cu(Bu <sub>2</sub> xantphos)(bpy)] <sup>+</sup>	384	652	0.3/0.4	—	584	3.0	1.95 <sup>f</sup>	597	7	—	< 1	27.6	—	< 1
[Cu(Bu <sub>2</sub> xantphos)(6-Mebpy)] <sup>+</sup>	382	605, 628sh	0.4/0.9	0.205/0.581	552	16	6.32 <sup>f</sup>	578	25	578	569	56.3	569	6
[Cu(Bu <sub>2</sub> xantphos)(6,6'-Me <sub>2</sub> bpy)] <sup>+</sup>	375	566 <sup>c</sup>	0.6/2.4 <sup>c</sup>	0.222/1.05 <sup>c</sup>	522	59	13.8 <sup>f</sup>	555	46	555	550	92.1	550	23
[Cu(xantphosMes <sub>2</sub> )(bpy)] <sup>+</sup>	385	655 <sup>c</sup>	0.2/0.2 <sup>c</sup>	—	589	1.9	1.19 <sup>f</sup>	594	11	594	594	20.0	594	< 1
[Cu(xantphosMes <sub>2</sub> )(6-Mebpy)] <sup>+</sup>	381	645, 623sh <sup>c</sup>	0.3/0.4 <sup>c</sup>	0.115/0.213	547	26	6.62 <sup>f</sup>	587	19	587	584	19.7	584	6
[Cu(xantphos)(bpy)] <sup>+</sup> <sup>d</sup>	383	620, 650	0.5/0.5	0.075/0.104	587	1.7	1.3	613	—	—	—	11	—	—
[Cu(xantphos)(6-Mebpy)] <sup>+</sup> <sup>e</sup>	379	635, 605	1.0/1.8	0.27/0.78	547	34	9.6	—	—	—	574	—	574	9.7.7
[Cu(xantphos)(6,6'-Me <sub>2</sub> bpy)] <sup>+</sup> <sup>e</sup>	378	635, 606	1.6/10	0.45/3.4	539	37	11	—	—	—	555	—	555	21.8

<sup>a</sup> Solution concentration = 2.5 × 10<sup>-5</sup> mol dm<sup>-3</sup> unless stated otherwise, sh = shoulder. <sup>b</sup> λ<sub>exc</sub> = 365 nm. <sup>c</sup> Solution concentration = 5.0 × 10<sup>-5</sup> mol dm<sup>-3</sup>. <sup>d</sup> Values taken from ref. 24. <sup>e</sup> Values taken from ref. 26. <sup>f</sup> Biexponential fit using the equation τ<sub>1/2</sub>(av) = ΣA<sub>i</sub>τ<sub>i</sub>/ΣA<sub>i</sub>, where A<sub>i</sub> is the pre-exponential factor for the lifetime.

**Table 4** Vertical excitation energies (*E*) calculated at the TD-DFT B3LYP/(def2svp + def2tzvp) level for the lowest singlet (S<sub>1</sub>) and triplet (T<sub>1</sub>) excited states of complexes [Cu(N<sup>^</sup>N)(P<sup>^</sup>AP)]<sup>+</sup> in CH<sub>2</sub>Cl<sub>2</sub> solution. Oscillator strengths (*f*) are given within parentheses for the S<sub>0</sub> → S<sub>1</sub> transition

Complex cation	S <sub>1</sub> <i>E</i> (eV nm <sup>-1</sup> ) ( <i>f</i> )	T <sub>1</sub> <i>E</i> (eV)
[Cu(xantphos)(bpy)] <sup>+</sup>	2.816/440 (0.08)	2.569
[Cu(Bu <sub>2</sub> xantphos)(bpy)] <sup>+</sup>	2.803/442 (0.09)	2.554
[Cu(Bu <sub>2</sub> xantphos)(6-Mebpy)] <sup>+</sup>	2.823/439 (0.10)	2.577
[Cu(Bu <sub>2</sub> xantphos)(6,6'-Me <sub>2</sub> bpy)] <sup>+</sup>	2.923/424 (0.07)	2.694
[Cu(xantphosMes <sub>2</sub> )(bpy)] <sup>+</sup>	2.664/465 (0.06)	2.470
[Cu(xantphosMes <sub>2</sub> )(6-Mebpy)] <sup>+</sup>	2.750/451 (0.06)	2.582

**Fig. 12** Normalized solid-state emission spectra of [Cu(P<sup>^</sup>AP)(N<sup>^</sup>N)](PF<sub>6</sub>) complexes (λ<sub>exc</sub> = 365 nm).

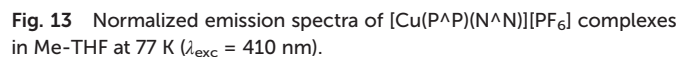
higher energies as more methyl groups are added to the bpy ligand (Table 4). The [Cu(Bu<sub>2</sub>xantphos)(6,6'-Me<sub>2</sub>bpy)]<sup>+</sup> complex is predicted to have the higher energy T<sub>1</sub>, followed by [Cu(Bu<sub>2</sub>xantphos)(6-Mebpy)]<sup>+</sup> and [Cu(xantphosMes<sub>2</sub>)(6-Mebpy)]<sup>+</sup>, and finally by the complexes with no methyl substituent. This is in good agreement with the emission wavelengths observed in experimental spectra (Table 3). The broad and mostly unstructured shape of the emission band (Fig. S24<sup>†</sup>) also agrees with the MLCT nature predicted for the emitting HOMO → LUMO T<sub>1</sub> state.

As discussed above, the geometry relaxation of the emitting T<sub>1</sub> state leads to the flattening of the tetrahedral coordination environment. This flattening is more hindered as the number of methyl substituents attached to positions 6 and 6' of the bpy ligand is increased, and the relaxation of the T<sub>1</sub> triplet is impeded thus leading to higher emission energies. Inspection of Table 3 shows that increasing the steric hindrance of the bpy ligand is beneficial for the emissive properties. Less flattening of the tetrahedral coordination environment of the copper centre gives rise to higher emission energies and, as

pared to the solid state emission and a greatly enlarged excited state lifetime. This indicates the possibility that all complexes are TADF emitters at room temperature. The energy difference between the lowest energy singlet and triplet excited states has been calculated to lie between 0.17 and 0.25 eV (Table 4), and is small enough to allow the occurrence of TADF processes.<sup>22</sup>

Low temperature data further support the idea that the position of the emission bands of the  $[\text{Cu}(\text{Bu}_2\text{xantphos})(\text{N}^-\text{N})]$  complexes is strongly affected by the flattening of the tetrahedral environment in the  $\text{T}_1$  state. In solution, this flattening is not impeded and the difference in peak position between  $[\text{Cu}(\text{Bu}_2\text{xantphos})(\text{bpy})][\text{PF}_6]$  and  $[\text{Cu}(\text{Bu}_2\text{xantphos})(6\text{-Mebpy})][\text{PF}_6]$  is 86 nm (0.30 eV) (Table 3). In powder, the flattening is more restricted and the difference decreases to 62 nm (0.25 eV). Finally, at 77 K, where the relaxation is even more impeded for all the complexes, the emission maxima range between 597 and 555 nm, in a window of just 42 nm (0.15 eV).

The series of compounds was tested in LECs using ITO/PEDOT:PSS as the anode, an emitting layer consisting of the complex in the presence of [Emim][PF<sub>6</sub>] (4 : 1 molar ratio) and an aluminium cathode. Devices were tested monitoring the electroluminescence and voltage over time, and were driven with a pulsed current (100 A m<sup>-2</sup> average, 50% duty cycle, 1 kHz). The main device parameters obtained for the entire samples series are reported in Table 5. The time evolution of the voltage and luminance for the LECs are reported in Fig. 14, together with the electroluminescence spectra. All LECs based on copper(II) complexes with <sup>t</sup>Bu<sub>2</sub>xantphos as the P^P ligand show a fast luminescence turn-on time (*t*<sub>on</sub>, defined here as the time to reach the maximum luminance), ranging from 1 minute for the complex with 6,6'-Me<sub>2</sub>bpy to 4.5 minutes for the one with 6-Mebpy (Fig. 14b). The maximum luminance registered for these compounds increases with increasing substitution to the N^N ligand, going from 20 cd m<sup>-2</sup> for the complex with unsubstituted bpy, to 230 cd m<sup>-2</sup> and 370 cd m<sup>-2</sup> for the ones containing 6-Mebpy and 6,6'-Me<sub>2</sub>bpy, respectively. This trend follows that of the PLQY registered for the same compounds (Table 3) and is consistent with an augmented steric hindrance of the N^N ligand, resulting in a higher stabilization of the tetrahedral complex geometry. The highest efficiency of 3.7 cd A<sup>-1</sup> for the LECs using [Cu(<sup>t</sup>Bu<sub>2</sub>xantphos)(6,6'-Me<sub>2</sub>bpy)][PF<sub>6</sub>] corresponds to an external quantum efficiency of 1.0%, which is substan-



$[\text{Cu}(\text{P}^{\wedge}\text{P})(\text{N}^{\wedge}\text{N})]^+$	$t_{\text{on}}$ (min)	$\text{Lum}_{\text{max}}$ ( $\text{cd m}^{-2}$ )	$t_{1/2}$ (min)	Eff. ( $\text{cd A}^{-1}$ )
$[\text{Cu}^f(\text{Bu}_2\text{xantphos})(\text{bpy})]^+$	1.1	20	5.1	0.2
$[\text{Cu}^f(\text{Bu}_2\text{xantphos})(6\text{-Meppy})]^+$	4.5	230	53.8	2.3
$[\text{Cu}^f(\text{Bu}_2\text{xantphos})(6,6'\text{-Me}_2\text{bpy})]^+$	1.0	370	4.9	3.7
$[\text{Cu}(\text{xantphosMes}_3)(6\text{-Meppy})]^+$	0.7	50	34.6	0.5



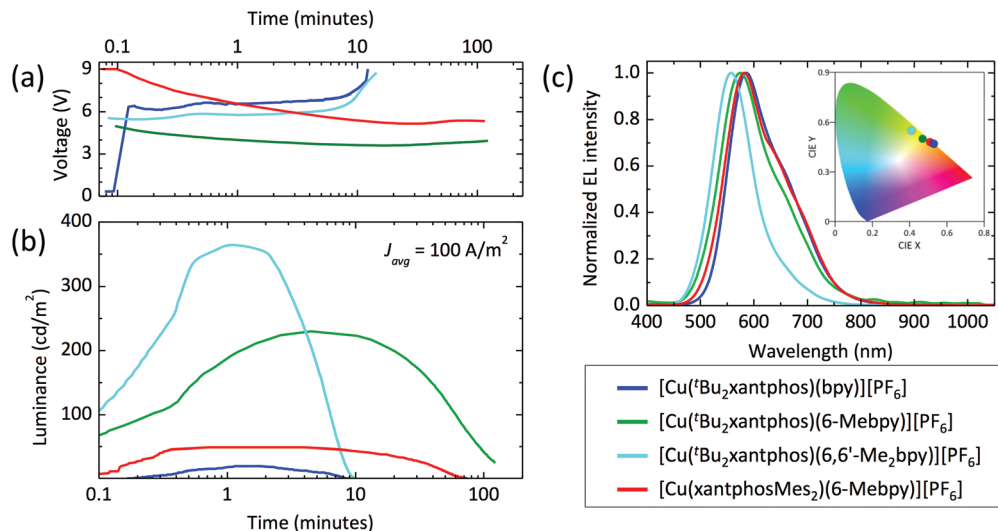


Fig. 14 Time evolution of the (a) voltage and (b) the luminance for a series of LECs driven at an average current density of  $100 \text{ A m}^{-2}$ . (c) Electroluminescence spectra for the same device series with (inset) the corresponding colour coordinates in the CIE 1931 colour space.

tially lower as compared to the PLQY of the same compound in thin-film (23%). This implies that even in such bright device, non-radiative losses dominate the recombination of the injected electrons and holes. Interestingly, the quantum efficiencies for photo- and electro-luminescence of the  $[\text{Cu}(\text{Bu}_2\text{xantphos})(6,6'\text{-Me}_2\text{bpy})][\text{PF}_6]$  are very close to the unsubstituted xantphos analogue (PLQY = 22% and maximum EQE = 1.0%),<sup>26</sup> highlighting the dominant role of the N<sup>N</sup> ligands on the optical and optoelectronic properties of these compounds.

In general, the device lifetime ( $t_{1/2}$ , time to decay to one-half of the peak luminance) for complexes containing  $\text{Bu}_2\text{xantphos}$  was found to be low, approximately 5 minutes in the cases of bpy and 6,6'-Me<sub>2</sub>bpy and above 50 minutes for the LECs with  $[\text{Cu}(\text{Bu}_2\text{xantphos})(6\text{-Mebpy})][\text{PF}_6]$ . The low lifetime of the complexes with bpy and 6,6'-Me<sub>2</sub>bpy might be due to a reduced stability of the materials toward charge transport, as seen from the corresponding LECs voltage profile which drastically increases after only few minutes of operation (Fig. 14a).

The optoelectronic performance of complexes containing the xantphosMes<sub>2</sub> ligand were in general lower as compared to those involving  $\text{Bu}_2\text{xantphos}$ . We could not observe any electroluminescence from  $[\text{Cu}(\text{xantphosMes}_2)(\text{bpy})][\text{PF}_6]$ , perhaps due to its low PLQY both in solution and in the solid state. Moderate electroluminescence was measured for  $[\text{Cu}(\text{xantphosMes}_2)(6\text{-Mebpy})][\text{PF}_6]$ , with fast turn-on (<1 minute) and a maximum luminance of  $50 \text{ cd m}^{-2}$ .

The spectral shape and position of the electroluminescence (EL, Fig. 14c) signals correlate with the PL maxima observed for the complexes in solution and in the solid state. For the  $\text{Bu}_2\text{xantphos}$ -containing complexes, the EL maxima blue-shift from 584 nm to 575 and 557 nm when increasing the substitution at the bpy, *i.e.* going from bpy to 6-Mebpy and 6,6'-Me<sub>2</sub>bpy, respectively. As highlighted in the inset of Fig. 14c, this shift corresponds to a colour variation from the orange to

the green region of the CIE 1931 colour space. The EL spectrum of  $[\text{Cu}(\text{xantphosMes}_2)(6\text{-Mebpy})][\text{PF}_6]$  peaks at 582 nm, in agreement with the PL signal of the thin-film (Table 3).

## Conclusions

We have prepared  $[\text{Cu}(\text{Bu}_2\text{xantphos})(\text{bpy})][\text{PF}_6]$ ,  $[\text{Cu}(\text{Bu}_2\text{xantphos})(6\text{-Mebpy})][\text{PF}_6]$ ,  $[\text{Cu}(\text{Bu}_2\text{xantphos})(6,6'\text{-Me}_2\text{bpy})][\text{PF}_6]$ ,  $[\text{Cu}(\text{xantphosMes}_2)(\text{bpy})][\text{PF}_6]$  and  $[\text{Cu}(\text{xantphosMes}_2)(6\text{-Mebpy})][\text{PF}_6]$ , but steric effects militate against the isolation of  $[\text{Cu}(\text{xantphosMes}_2)(6,6'\text{-Me}_2\text{bpy})][\text{PF}_6]$ . To prepare the latter, the chiral xantphosMes<sub>2</sub> was prepared and characterized, and the single crystal structure reveals the presence of the (*rac*)-form. In solution, one dominant diastereoisomer is observed, proposed as the (*rac*) rather than the (*meso*)-form. This makes the bisphosphane preorganized to give particular diastereoisomers when coordinated to copper(I) in  $[\text{Cu}(\text{xantphosMes}_2)(\text{N}^{\wedge}\text{N})]^+$  complexes. Single crystal structures of four complexes were determined. In  $[\text{Cu}(\text{xantphosMes}_2)(6\text{-Mebpy})][\text{PF}_6]$ , the 6-Mebpy unit is disordered over two orientations with 50% occupancies. The disorder corresponds to a combination of two dynamic processes, which the  $[\text{Cu}(\text{xantphosMes}_2)(\text{N}^{\wedge}\text{N})]^+$  cations undergo in solution. DFT calculations reveal that the energy difference between the two conformers observed in the solid-state structure differ only by  $0.28 \text{ kcal mol}^{-1}$ .

The  $[\text{Cu}(\text{P}^{\wedge}\text{P})(\text{N}^{\wedge}\text{N})][\text{PF}_6]$  compounds show a broad MLCT-absorption around 380 nm which shifts to higher energies on going from bpy to 6-Mebpy to 6,6'-Me<sub>2</sub>bpy. Upon excitation into the MLCT band, the  $[\text{Cu}(\text{P}^{\wedge}\text{P})(\text{N}^{\wedge}\text{N})][\text{PF}_6]$  complexes emit in the yellow to orange region; additional Me groups in the bpy ligand result in a blue-shift in the emission. The MLCT nature of the absorption and emission is supported by DFT calculations, which associate the lowest-energy S<sub>1</sub> and T<sub>1</sub> excited states to the HOMO → LUMO monoexcitation implying



an electron transfer from the Cu(P<sup>^</sup>P) moiety to the bpy ligand. In solution, PLQY values are low, but in the solid state, PLQYs of 26 and 59% are observed for [Cu(xantphosMes<sub>2</sub>)(6-Mebpy)][PF<sub>6</sub>] and [Cu(<sup>t</sup>Bu<sub>2</sub>xantphos)(6,6'-Me<sub>2</sub>bpy)]<sup>+</sup>, respectively, compared to benchmark values of 34 and 37% for [Cu(xantphos)(6-Mebpy)][PF<sub>6</sub>] and [Cu(xantphos)(6,6'-Me<sub>2</sub>bpy)][PF<sub>6</sub>]. Increased excited state lifetimes at low temperature are consistent with the complexes being TADF emitters and this is supported by a calculated energy difference between S<sub>1</sub> and T<sub>1</sub> of 0.17–0.25 eV.

The compounds were tested in simple bilayer LECs. The optoelectronic performance of complexes containing the xantphosMes<sub>2</sub> ligand were generally lower than those with <sup>t</sup>Bu<sub>2</sub>xantphos, which led to bright and efficient devices. The current efficiency of the LECs follows the trend observed for the PLQY, increasing with increasing substitution at the bpy ligand. In particular, luminances as high as 370 cd m<sup>-2</sup> were obtained for the complex [Cu(<sup>t</sup>Bu<sub>2</sub>xantphos)(6,6'-Me<sub>2</sub>bpy)][PF<sub>6</sub>], which correspond to an efficiency of 3.7 cd A<sup>-1</sup>. These encouraging results suggest that <sup>t</sup>Bu<sub>2</sub>xantphos is a promising ligand to develop novel and efficient copper emitters for LECs and OLEDs.

## Conflicts of interest

There are no conflicts to declare.

## Acknowledgements

Financial support from the Swiss National Science Foundation (Grant number 162631), the University of Basel, the MINECO of Spain (CTQ2015-71154-P, MAT2017-88821-R and Unidad de Excelencia María de Maeztu MDM-2015-0538), the Generalitat Valenciana (PROMETEO/2016/ 135) and European FEDER funds (CTQ2015-71154-P) is acknowledged. Prof. Dr Oliver S. Wenger and Dr Christopher B. Larsen (University of Basel) are thanked for the use of the LP920-KS instrument from Edinburgh Instruments for low-temperature emission and lifetime measurements. MS thanks the MINECO for his RyC contract. Dr Sarah Keller is acknowledged for fruitful discussions and synthetic assistance. Kenneth Atz and PD Dr Daniel Häussinger are acknowledged for assistance with variable temperature NMR measurements.

## Notes and references

- M. Y. Wong and E. Zysman-Colman, *Adv. Mater.*, 2017, **29**, 1605444.
- C. Bizzarri, E. Spuling, D. M. Knoll, D. Volz and S. Bräse, *Coord. Chem. Rev.*, 2018, **373**, 49.
- D. Volz, M. Wallesch, C. Fléchon, M. Danz, A. Verma, J. M. Navarro, D. M. Zink, S. Bräse and T. Baumann, *Green Chem.*, 2015, **17**, 1988.
- E. Fresta and R. D. Costa, *J. Mater. Chem. C*, 2017, **5**, 5643.
- S. Tang and L. Edman, *Top. Curr. Chem.*, 2016, **374**, 40.
- J. Wu, F. Li, Q. Zeng, C. Nie, P. C. Ooi, T. Guo, G. Shan and Z. Su, *Org. Electron.*, 2016, **28**, 314.
- A. Sandström and L. Edman, *Energy Technol.*, 2015, **3**, 329.
- Light-emitting electrochemical cells: Concepts, advances and challenges*, ed. R. D. Costa, Springer, Cham, 2017.
- R. D. Costa, E. Ortí, H. J. Bolink, F. Monit, G. Accorsi and N. Armaroli, *Angew. Chem., Int. Ed.*, 2012, **51**, 8178.
- C. E. Housecroft and E. C. Constable, *Coord. Chem. Rev.*, 2017, **350**, 155.
- A. M. Bünzli, E. C. Constable, C. E. Housecroft, A. Prescimone, J. A. Zampese, G. Longo, L. Gil-Escrig, A. Pertegás, E. Ortí and H. J. Bolink, *Chem. Sci.*, 2015, **6**, 2843.
- D. Tordera, A. M. Bünzli, A. Pertegás, J. M. Junquera-Hernández, E. C. Constable, J. A. Zampese, C. E. Housecroft, E. Ortí and H. J. Bolink, *Chem. – Eur. J.*, 2013, **19**, 8597.
- S. B. Meier, D. Tordera, A. Pertegás, C. Roldán-Carmona, E. Ortí and H. J. Bolink, *Mater. Today*, 2014, **17**, 217.
- B. N. Bideh, C. Roldán-Carmona, H. Shahroosvand and M. K. Nazeeruddin, *Dalton Trans.*, 2016, **45**, 7195.
- M. T. Buckner and D. R. McMillin, *J. Chem. Soc., Chem. Commun.*, 1978, 759.
- R. A. Rader, D. R. McMillin, M. T. Buckner, T. G. Matthews, D. J. Casadonte, R. K. Lengel, S. B. Whittaker, L. M. Darmon and F. E. Lytle, *J. Am. Chem. Soc.*, 1981, **103**, 5906.
- C. L. Linfoot, M. J. Leidl, P. Richardson, A. F. Rausch, O. Chepelin, F. J. White, H. Yersin and N. Robertson, *Inorg. Chem.*, 2014, **53**, 10854.
- M. J. Leidl, V. a. Krylova, P. I. Djurovich, M. E. Thompson and H. Yersin, *J. Am. Chem. Soc.*, 2014, **136**, 16032.
- R. Czerwieniec and H. Yersin, *Inorg. Chem.*, 2015, **54**, 4322.
- T. Hofbeck, U. Monkowius and H. Yersin, *J. Am. Chem. Soc.*, 2015, **137**, 399.
- R. Czerwieniec, M. J. Leidl, H. H. H. Homeier and H. Yersin, *Coord. Chem. Rev.*, 2016, **325**, 2.
- H. Yersin, R. Czerwieniec, M. Z. Shafikov and A. F. Suleymanova, *ChemPhysChem*, 2017, **18**, 3508.
- J. Liu, J. Oliva, K. Tong, F. Zhao, D. Chen and Q. Pei, *Sci. Rep.*, 2017, **7**, 1524.
- S. Keller, F. Brunner, J. M. Junquera-Hernández, A. Pertegás, M.-G. La-Placa, A. Prescimone, E. C. Constable, H. J. Bolink, E. Ortí and C. E. Housecroft, *ChemPlusChem*, 2018, **83**, 217.
- S. Keller, E. C. Constable, C. E. Housecroft, M. Neuburger, A. Prescimone, G. Longo, A. Pertegás, M. Sessolo and H. J. Bolink, *Dalton Trans.*, 2014, **43**, 16593.
- S. Keller, A. Pertegás, G. Longo, L. Martínez, J. Cerdá, J. M. Junquera-Hernández, A. Prescimone, E. C. Constable, C. E. Housecroft, E. Ortí and H. J. Bolink, *J. Mater. Chem. C*, 2016, **4**, 3857.
- M. D. Weber, M. Viciano-Chumillas, D. Armentano, J. Cano and R. D. Costa, *Dalton Trans.*, 2017, **46**, 6312.
- E. Fresta and R. D. Costa, *J. Mater. Chem. C*, 2017, **5**, 5643.



- 29 M. Heberle, S. Tschierlei, N. Rockstroh, M. Ringenberg, W. Frey, H. Junge, M. Beller, S. Lochbrunner and M. Karnahl, *Chem. – Eur. J.*, 2017, **23**, 312.
- 30 N. Armaroli, G. Accorsi, M. Holler, O. Moudam, J.-F. Nierengarten, Z. Zhou, R. T. Wegh and R. Welter, *Adv. Mater.*, 2006, **18**, 1313.
- 31 F. Brunner, L. Martínez-Sarti, S. Keller, A. Pertegás, A. Prescimone, E. C. Constable, H. J. Bolink and C. E. Housecroft, *Dalton Trans.*, 2016, **45**, 15180.
- 32 F. Brunner, S. Graber, Y. Baumgartner, D. Häussinger, A. Prescimone, E. C. Constable and C. E. Housecroft, *Dalton Trans.*, 2017, **46**, 6379.
- 33 C. Yi, S. Xu, J. Wang, F. Zhao, H. Xia and Y. Wang, *Eur. J. Inorg. Chem.*, 2016, **2016**, 4885.
- 34 R. Czerwieniec, J. Yu and H. Yersin, *Inorg. Chem.*, 2011, **50**, 8293.
- 35 Q. Zhang, Q. Zhou, Y. Cheng, L. Wang, D. Ma, X. Jing and F. Wang, *Adv. Funct. Mater.*, 2006, **16**, 1203.
- 36 R. D. Costa, D. Tordera, E. Ortí, H. J. Bolink, J. Schönle, S. Graber, C. E. Housecroft, E. C. Constable and J. A. Zampese, *J. Mater. Chem.*, 2011, **21**, 16108.
- 37 S. Keller, A. Prescimone, E. C. Constable and C. E. Housecroft, *Photochem. Photobiol. Sci.*, 2018, **17**, 375.
- 38 A. M. Johns, N. Sakai, A. Ridder and J. F. Hartwig, *J. Am. Chem. Soc.*, 2006, **128**, 9306.
- 39 C. A. Tolman, *Chem. Rev.*, 1977, **77**, 313.
- 40 G. J. Kubas, *Inorg. Synth.*, 1979, **19**, 90.
- 41 W. Bruker Analytical X-ray Systems, Inc., *APEX2, version 2 User Manual*, M86-E01078, Madison, 2006.
- 42 P. W. Betteridge, J. R. Carruthers, R. I. Cooper, K. Prout and D. J. Watkin, *J. Appl. Crystallogr.*, 2003, **36**, 1487.
- 43 I. J. Bruno, J. C. Cole, P. R. Edgington, M. Kessler, C. F. Macrae, P. McCabe, J. Pearson and R. Taylor, *Acta Crystallogr., Sect. B: Struct. Sci.*, 2002, **58**, 389.
- 44 C. F. Macrae, I. J. Bruno, J. A. Chisholm, P. R. Edgington, P. McCabe, E. Pidcock, L. Rodriguez-Monge, R. Taylor, J. van de Streek and P. A. Wood, *J. Appl. Crystallogr.*, 2008, **41**, 466.
- 45 A. L. Spek, *Acta Crystallogr., Sect. C: Struct. Chem.*, 2015, **71**, 9.
- 46 M. J. Frisch, G. W. Trucks, H. B. Schlegel, G. E. Scuseria, M. A. Robb, J. R. Cheeseman, G. Scalmani, V. Barone, G. A. Petersson, H. Nakatsuji, X. Li, M. Caricato, A. V. Marenich, J. Bloino, B. G. Janesko, R. Gomperts, B. Mennucci, H. P. Hratchian, J. V. Ortiz, A. F. Izmaylov, J. L. Sonnenberg, D. Williams-Young, F. Ding, F. Lipparini, F. Egidi, J. Goings, B. Peng, A. Petrone, T. Henderson, D. Ranasinghe, V. G. Zakrzewski, J. Gao, N. Rega, G. Zheng, W. Liang, M. Hada, M. Ehara, K. Toyota, R. Fukuda, J. Hasegawa, M. Ishida, T. Nakajima, Y. Honda, O. Kitao, H. Nakai, T. Vreven, K. Throssell, J. A. Montgomery Jr., J. E. Peralta, F. Ogliaro, M. J. Bearpark, J. J. Heyd, E. N. Brothers, K. N. Kudin, V. N. Staroverov, T. A. Keith, R. Kobayashi, J. Normand, K. Raghavachari, A. P. Rendell, J. C. Burant, S. S. Iyengar, J. Tomasi, M. Cossi, J. M. Millam, M. Klene, C. Adamo, R. Cammi, J. W. Ochterski, R. L. Martin, K. Morokuma, O. Farkas, J. B. Foresman and D. J. Fox, *Gaussian 16, Revision A.03*, Gaussian, Inc., Wallingford CT, 2016.
- 47 C. Lee, W. Yang and R. G. Parr, *Phys. Rev. B: Condens. Matter Mater. Phys.*, 1988, **37**, 785.
- 48 A. D. Becke, *J. Chem. Phys.*, 1993, **98**, 5648.
- 49 F. Weigend and R. Ahlrichs, *Phys. Chem. Chem. Phys.*, 2005, **7**, 3297.
- 50 F. Weigend, *Phys. Chem. Chem. Phys.*, 2006, **8**, 1057.
- 51 S. Grimme, J. Antony, S. Ehrlich and H. Krieg, *J. Chem. Phys.*, 2010, **132**, 154104.
- 52 S. Grimme, S. Ehrlich and L. Goerigk, *J. Comput. Chem.*, 2011, **32**, 1456.
- 53 M. Petersilka, U. J. Gossmann and E. K. U. Gross, *Phys. Rev. Lett.*, 1996, **76**, 1212.
- 54 C. Jamorski, M. E. Casida and D. R. Salahub, *J. Chem. Phys.*, 1996, **104**, 5134.
- 55 M. E. Casida, C. Jamorski, K. C. Casida and D. R. Salahub, *J. Chem. Phys.*, 1998, **108**, 4439.
- 56 J. Tomasi and M. Persico, *Chem. Rev.*, 1994, **94**, 2027.
- 57 C. J. Cramer and D. G. Truhlar, in *Solvent Effects and Chemical Reactivity*, ed. O. Tapia and J. Bertrán, Kluwer, 1996, pp. 1–80.
- 58 J. Tomasi, B. Mennucci and R. Cammi, *Chem. Rev.*, 2005, **105**, 2999.
- 59 B. C. Hamann and J. F. Hartwig, *J. Am. Chem. Soc.*, 1998, **120**, 3694.
- 60 J. Holz, K. Rumpel, A. Spannenberg, R. Paciello, H. Jiao and A. Börner, *ACS Catal.*, 2017, **7**, 6162.
- 61 Y. Hamada, F. Matsuura, M. Oku, K. Hatano and T. Shioiri, *Tetrahedron Lett.*, 1997, **38**, 8961.
- 62 J. I. van der Vlugt, E. A. Pidko, D. Vogt, M. Lutz and A. L. Spek, *Inorg. Chem.*, 2009, **48**, 7513.
- 63 J. Yuasa, M. Dan and T. Kawai, *Dalton Trans.*, 2013, **42**, 16096.
- 64 B. Bozic-Weber, V. Chaurin, E. C. Constable, C. E. Housecroft, M. Meuwly, M. Neuburger, J. A. Rudd, E. Schönhofner and L. Siegfried, *Dalton Trans.*, 2012, **41**, 14157.
- 65 C. R. Groom, I. J. Bruno, M. P. Lightfoot and S. C. Ward, *Acta Crystallogr., Sect. B: Struct. Sci., Cryst. Eng. Mater.*, 2016, **72**, 171.
- 66 S. Keller, A. Prescimone, H. Bolink, M. Sessolo, G. Longo, L. Martínez-Sarti, J. M. Junquera-Hernández, E. C. Constable, E. Ortí and C. E. Housecroft, *Dalton Trans.*, 2018, **47**, 14263.

